'1989A&A...215..347C'

Astron. Astrophys. 215, 347–359 (1989)

ASTRONOMY AND ASTROPHYSICS

SNR expansion in a pre-existent cavity

L. Ciotti and A. D'Ercole

Osservatorio Astronomico di Bologna, C.P. 596, I-40100 Bologna, Italy

Received July 28, accepted October 17, 1988

Summary. Supernova ejecta created by the explosion of an O-B star are expected to expand through a pre-existing bubble generated by the previous fast stellar wind. In order to study the interaction between such a bubble and the supernova remnant with an appreciable spatial resolution, we performed two separate numerical computations making use of moving grids. We first simulated the bubble evolution until the steady state was reached. Then we simulated the supernova remnant expansion in such a way as to obtain the Chevalier solution as long as the remnant itself travels through the unperturbed wind. Finally the remnant merged in the bubble, whose presence was recognized through the boundary conditions at the outer side of the remnant grid. It turns out that the geometry of ring-like supernova remnants such as the Cygnus Loop can be readily understood. For closer comparisons with observational data, however, the red giant phase of the progenitor must be considered. During this stage the gas of the bubble moves inward while a rarefaction wave travels through the bubble cooling it.

Key words: hydrodynamics – interstellar medium: bubbles – interstellar medium: H II regions: general – supernovae and supernova remnants: general

1. Introduction

It is believed that the progenitors of Type II supernovae (SN) are massive stars ($M > 8\,M_\odot$) which spend most of their life as blue supergiants (BSG). Such supergiants suffer a concrete mass loss through a fast wind ($V_w \sim 2000\,\mathrm{km\,s^{-1}}$) at a rate $\dot{M} = 10^{-7} \div 10^{-6}\,M_\odot\,\mathrm{yr}^{-1}$. The last 10 percent of their life is spent as red supergiants (RSG) which possess strong slow winds with $\dot{M}$ of the order of $10^{-6} \div 10^{-5}\,M_\odot\,\mathrm{yr}^{-1}$ and velocities $V_w \sim 10\,\mathrm{km\,s^{-1}}$. For massive, luminous stars ($M > 10-20\,M_\odot$) with high mass loss rate, the star can loose most of its outer hydrogen rich envelope before the carbon burning stage, so instead of ending its life as an RSG, it may explode as a compact, hot Wolf-Rayet (WR) star with little hydrogen.

In any case the ejecta of young Type II supernova remnants (SNRs) are likely to expand in a circumstellar medium (CSM) whose density profile decreases as r^{-2}, if $\dot{M}$ and V_w are supposed to be constant and isotropic. The structure of the remnant depends on the importance of cooling in the gas. In the case of an adiabatic shock Chevalier similarity solutions (Chevalier, 1982) give the behaviour. However, the power law density distribution of the CSM cannot hold at large distances; assuming that the RSG stage lasts 10^5 yr, the slow wind cannot extend more than 1 pc. Inside this distance the SNR expansion follows the Chevalier solution, but later, when the shock reaches the interstellar medium (ISM), a pair of shocks are formed as a result of the expansion into the low density medium (Itoh and Fabian, 1984). The assumption that the ISM is uniform at the neighbourhood of the slow wind is however quite rude; more sporadic, short-lived mass ejections are in fact expected during the carbon burning phase or at later phases, due to the shell flashes, similar to those suggested to be responsible for planetary nebulae. Moreover, the fast wind blown during the BSG phase pushes the ISM away producing an expanding bubble of hot gas ($T \sim 10^6$ K) at low density ($n \sim 10^{-2}\,\mathrm{cm^{-3}}$) confined between an outward driven and a reflected shock (cf. Weaver et al., 1977). Such a bubble is likely to become stationary after few million years (if the star exists this long). At this time it extends over some tens of parsecs all around the star and it is bounded at the outer edge by the cooler ($T \sim 8000$ K) surrounding H II region. The inner shock is located some parsec far from the star and its pressure is balanced by the dynamical pressure of the fast wind.

While observational data support the idea of some SNR interacting with a preexisting cavity (Braun et al., 1986a, b), little theoretical work has been done to describe such an interaction. This paper represents a first attempt in this direction. The problem is quite complex and a number of simplifying assumptions must be done in order to render the problem tractable. The most important (and limiting) hypothesis regards the bubble, which is assumed to remain stationary until the SN explodes. This comes from the fact that we calculated separately the bubble development and the subsequent SNR expansion in order to get an appreciable spatial resolution. Actually, a back-filling is expected when the star moves from the BSG to the RSG region and the fast wind ceases; in other words the hot gas of the bubble, no more confined at the inner radius by the ram pressure of the BSG wind, moves toward the centre while a rarefaction wave crosses the bubble itself. To avoid this complication we assumed that a fast wind blows during all the star life; this in turn implies that our model is valid only for SN progenitors which never moved from the blue region of the H-R diagram. Despite its severity, this assumption does not affect the overall SNR dynamical behaviour. Our present results represent therefore a guideline for more general cases.

In Sect. 2 we discuss the problem of the "ever blue" progenitors. In Sects. 3 and 4 hypotheses and hydrodynamics concerning the bubble and the SNR are summarized. Section 5

Send offprint requests to: A. D'Ercole

© European Southern Observatory • Provided by the NASA Astrophysics Data System

'1989A&A...215..347C'

describes our numerical approach to the problem. Finally, in Sects. 6 and 7 results are presented and discussed, while merits and limits of the model are summarized in Sect. 8.

2. The supernova progenitor

It is well known that mass loss affects star evolution for star initial masses greater than 8 $M_\odot$ (Maeder, 1981). The main effect of mass loss is to shift the evolutionary tracks in the HR diagram to lower luminosity and effective temperature. In particular, we are concerned here with the location of the supernovae precursors. Conservatory evolutionary models end their evolution as red supergiants for any value of the stellar mass. However mass loss makes the supernova precursors, which have an initial mass greater than some threshold value, move from RSG back to the blue; these stars are likely to correspond to Wolf-Rayet (WR) stars. This behaviour seems in fact confirmed by the strong anticorrelation observed between RSG and WR stars in the galaxy: red supergiants progressively become quite rare in the HR diagram at the same luminosity above which WR stars appear. The time spent by a star in the RSG phase is shorter for higher mass loss rates. It may be that the massive stars (which suffer the higher mass loss) skip the RSG stage entirely, and become WR stars (cf. Maeder, 1983). Actually the brightest red supergiants are not as luminous as the most luminous blue supergiants, suggesting that there must be some upper limit above which stars do not become red supergiants (cf. Humphreys and Nichols, 1985). Following Chiosi and Maeder (1986), we can schematize the situation as follows: a) stars with initial masses in the range $8 \div 25\, M_\odot$ explode as RSG; b) for stars with initial masses $25\, M_\odot < M < 60\, M_\odot$ the high stellar winds in the red supergiant stage progressively remove the outer envelope and the star then may evolve to the blue, depending on the efficiency of the mass loss; c) finally, for stars with initial masses larger than 60 $M_\odot$, the winds responsible for the peeling during the main sequence and early shell H-burning phases are high enough to remove all stellar outer layers and a bare He core is left over. This prevents any evolution towards the red supergiant stage and thus the stars are always blue.

As outlined in Sect. 1, and as it will become clearer later, in order to reduce our problem to an acceptable level of complexity we assumed that the bubble generated by the wind of the progenitor star remains stationary until the supernova explosion. From the above discussion, this means that our model can be considered realistic for stars with initial masses above 60 $M_\odot$, or for stars with an initial mass lower than this but with a negligible fraction of their life spent as RSG (see however Sect. 7).

Before concluding this Section, we want to point out that the above reasoning changes somewhat if different stellar metallicities Z are considered. Brunish and Truran (1982), on the assumption that metallicity does not affect *directly* the mass loss rate (this assumption is however questioned by Chiosi and Maeder, 1986) find that the lower the metal content, the bluer the model appears. Because of this effect, the total amount of mass lost by lower Z models is higher. It turns out that stars with an initial mass $M = 15\, M_\odot$ are never red for metallicity $Z = 0.001$, and spend only $4\,10^4$ yr in the RSG stage for $Z = 0.01$. These models present mass loss rates between one and two order of magnitude lower than $10^{-6}\, M_\odot\ \mathrm{yr}^{-1}$, which is the value we adopted to simulate numerically the bubble. However it results that all the models with an initial mass $M \geq 30\, M_\odot$ and $0.01 > Z > 0.0002$ have an acceptable mass loss rate and spend only few tens of thousand years as RSG. Similar conclusions are reached by Hillebrandt et al. (1987). Adopting $Z = Z_G/4$ and $Z = Z_G/10$ for the Large and Small Magellanic Cloud respectively ($Z_G = 0.03$), we can expect that our computations find a larger statistical application in these galaxies; in fact "ever blue" SN progenitors have smaller masses and are therefore more numerous.

3. The bubble

3.1. The model

The behaviour of stellar bubbles has already been studied by several authors (Avedisova, 1972; Castor et al., 1975; Falle, 1975; Steigman et al., 1975; Weaver et al., 1977) under a number of simplifying assumptions: (a) the ambient ISM has a uniform density ρ_0; (b) the star is at rest relative to the ISM; (c) the stellar wind is isotropic (i.e. there is spherical symmetry); (d) the mechanical luminosity of the wind, $L_w = \dot{M} V_w^2/2$, is constant.

The wind blown by the giant star pushes the interstellar medium away giving rise to a bubble bounded by an inward and outward driven shocks. The interior of the bubble is confined between the reverse shock in R_1 and the contact surface in R_c separating the shocked wind from the interstellar material. This volume is filled with hot ($T > 10^6$ K) shocked stellar wind at low density, while the swept-up interstellar gas is compressed by the outward driven shock in R_2, giving rise to a spherical shell. Part of the shell material, however, evaporates into the cavity via heat conduction. In fact the conduction front, initially at the contact between the stellar wind and the CSM, advances in the cool gas that in turn starts to evaporate. The conduction front moves forward and R_c then represents just a surface comoving with the fluid.

After an adiabatic expansion stage lasting a few thousand years, the swept-up interstellar gas collapses into a much thinner, cold shell as a result of radiative cooling. In the beginning of this snowplow phase the radiative losses of the hot interior are negligible, but after some hundred thousand years they become more and more important (especially in a small radius range close to the heat conduction front, where density and temperature have opposite gradients). In this phase the mass of the hot cavity coming from the shell evaporation overwhelms the mass that comes from the star, although the depletion of the mass of the cold shell is negligible. This shell is so thin that the radius R_b of the conduction front can be confused with R_2.

In few million years the pressure of the gas inside the expanding cavity decreases and eventually reaches the value of the pressure of the external H II region maintained at a temperature $T \sim 8000$ K by the central star. At this point the bubble stalls. In other words, the radius R_b of the conduction front stops to grow while almost all the wind luminosity L_w is radiated away. The outer shell dissipates into the surrounding medium as the external shock tends to become sonic.

We point out that in general pressure equilibrium and radiative losses have different time-scales and do not have to be coincident in time. In the case of momentum-conserving bubbles (Steigman et al., 1975), for instance, where radiative losses become important quite soon, cooling in the hot cavity is higher than L_w and the pressure drops. The inner region is therefore collapsed and $R_1 \sim R_2$; the stellar wind collides directly with the outer shell. In this case the bubble stalls when the ram pressure of the wind

© European Southern Observatory • Provided by the NASA Astrophysics Data System

'1989A&A...215..347C'

equals the external pressure, much later than the onset of the cooling. In general, if cooling is initially negligible, the hot cavity is created as stated before. The outer shell, which is decelerating, develops a slight positive pressure gradient with the pressure at the inner boundary of the shell lower than the pressure immediately behind R_2. Because of radiative cooling, a density gradient with opposite signature also develops and the shell itself is likely to be Rayleigh-Taylor instable. The influence of this instability is regulated by the presence of magnetic fields in the shell which are expected to freeze the instability itself (Bychkov, 1980). Injection of cool material into the bubble through breaches open in the shell increases the cooling rate and lowers the pressure. In reality, therefore, the onset of substantial radiative cooling and pressure equilibrium with the external H II region are likely to be contemporary.

In the following we will focus our attention to the energy-conserving bubbles (in which the thermal energy of the shocked wind is conserved during a non negligible fraction of the time-life) in order to compare our results with the solution given by Weaver et al. (1977).

3.2. *The numerical simulation*

In order to describe the interaction of a SNR with the bubble, we first reproduced numerically the results of Weaver et al. (1977) that we briefly summarized above. We solved the usual set of hydrodynamic equations:

$$\frac{\partial \rho}{\partial t}+\nabla\cdot(\rho v)=0, \tag{1a}$$

$$\frac{\partial m}{\partial t}+\nabla\cdot(mv)=-(\gamma-1)\nabla E, \tag{1b}$$

$$\frac{\partial E}{\partial t}+\nabla\cdot(Ev)=-(\gamma-1)E\nabla\cdot v-\nabla\cdot q-L, \tag{1c}$$

where ρ, m, E represent the density of mass, momentum and internal energy respectively, and v is the fluid velocity. The ratio of the specific heats is taken to be $\gamma=5/3$.

The cooling rate per unit volume is given by

$$L=n_e n_H(\Phi(T)-\Phi(T_0)), \tag{2}$$

where n_H and n_e are the number densities of hydrogen and electrons respectively, while T is the temperature. $\Phi(T)$ represents the cooling law. We adopt $\Phi(T)$ given by Kafatos (1973) who considered the effects of non-equilibrium ionization during the cooling of a low density optically thin gas with Aller's abundances (1961). We are assuming that the ambient gas is maintained at a uniform temperature $T_0=10^4$ K by stellar radiation. The heating term in Eq. (2) permits to avoid to solve the radiative transfer equation, but it is not satisfactory in presence of cold gas compression.

The heat flux is given by

$$q=-k\nabla T(1+k\nabla T/q_s)^{-1}. \tag{3}$$

When $k\nabla T/q_s \ll 1$ Eq. (3) becomes the classical formula of Spitzer (1962)

$$q=-k\nabla T, \tag{4}$$

where $k=0.6\ 10^{-6}\ T^{5/2}$ is the usual heat conduction coefficient in c.g.s. units. If, however, ∇T becomes too large, then the heat flux is limited by the value of the saturated flux q_s (see below for a deeper discussion).

3.3. *The hydrodynamic assumption*

The question may be raised whether the usual gasdynamical equations are meaningful in describing the bubble. The mean free path in the plasma, in fact, is given by

$$\lambda\sim 10^4\ T^2/n \text{ cm}. \tag{5}$$

At $t\sim 2\ 10^6$ yr, $R_1=9.5$ pc, $T=3\ 10^6$ K and $n=10^{-2}$ cm^{-3}, and we get $\lambda\sim 3$ pc. The inner shock thickness results therefore not negligible in front of R_1, and the situation is even worst at earlier times, when the temperature is higher. In actuality, the shock front is supposed to be collisionless. If a magnetic field is present, the shock thickness will be not much greater then the proton gyroradius $r_L\sim 10^{-4}\ v/B$ cm (where the fluid velocity v is normal to the magnetic field B); for a typical value of interstellar fields ($\sim 10^{-6}$ Gauss) we have $r_L\sim 10^{10}$ cm. In absence of the magnetic field, one might expect a turbulent electrostatic shock as discussed by McKee (1974). In this case the shock thickness would be of the order of the wind speed divided by the proton plasma frequency; this distance is about 10^9 cm in our case. It results therefore that in any case the thickness of the collisionless shock is small enough to be neglected.

Moreover, Cowie and McKee (1977) have suggested, from considerations on solar wind observations, that even when λ is larger than the fluid scale length the particle distribution function is still sufficiently isotropic because of the plasma instabilities. From all the above, it can be concluded that the hydrodynamic approximation is valid and we are allowed to use the usual gasdynamic equations [Eqs. (1a)–(1c)].

3.4. *The heat conduction*

In presence of large temperature gradients Eq. (4) can predict an energy flux greater than that actually carried by electrons. The maximum allowable energy flux (the saturated flux) is given by (Cowie and McKee, 1977)

$$q_s=\beta\varepsilon_e v_T, \tag{6}$$

where $\varepsilon_e=1.5n_e k_B T$, $v_T=(3k_B T/m_e)^{1/2}$ and k_B are the internal energy, the thermal velocity and the Boltzmann constant respectively. Estimates of β are uncertain. Following Cowie and McKee (1977) we choose $\beta=0.12$; this value is in good agreement both with observational data (Feldman et al., 1974) and theoretical estimates (Campbell, 1984).

The reason for the presence of a factor $\beta<1$ in Eq. (6) comes from the fact that in a collisionless plasma (where the saturated flux is usually effective) a significant number of plasma instabilities may develop, impeding the free flux of electrons at velocity v_T. A further reduction of q is given by magnetic fields in the direction normal to the field lines (Cowie and McKee, 1977). The effectiveness of magnetic fields and plasma turbulences in limiting the heat conduction is not known at present. For this reason, and also in order to compare our numerical results with the semi-analytical solution given by Weaver et al. (1977) (who consider Eq. (3) without any reduction in the value of k) we ignore their effects.

Another problem connected with the thermal conduction in plasmas is given by the heat transfer through discontinuities such

© European Southern Observatory • Provided by the NASA Astrophysics Data System

'1989A&A...215..347C'

as shocks and contact surfaces. When a shock propagates into a collisional gas, the heated electrons in the post-shock region acquire a thermal velocity that may be several times higher than the shock velocity itself (Zel'dovich and Raizer, 1967). These electrons, therefore, tend to overtake the shock front heating the upstream gas. If the same happened in collisionless shocks, then the young SNRs would show an X-ray emitting region larger than the remnant itself (Chevalier, 1975). This however is in contrast with the observations which indicate that the hot electrons are confined to the interior of the shock. It seems reasonable that the suppression of the heat flux is due to the highly turbulent regime at the shock front. For this reason we inhibited the heat conduction through the shock in R_1 (there is no temperature gradient in R_2, so that no conduction occurs there).

On the contrary, the heat conduction through the contact surface is not expected to be suppressed by the magnetic field frozen in the outer shell, because any magnetic field stretches in the radial direction as the gas evaporates between the two regions (Cowie and McKee, 1977; Cowie, 1977).

3.5. *Clumps in the bubble*

As pointed out before, the bubble model previously outlined holds in the case of homogeneous ambient media. The interstellar medium, however, is known to have an inhomogeneous structure with a large range of densities. This is expected to have important consequences on the bubble dynamics (and cooling). The bubble evolution in a cloudy medium generated by a B0 star or earlier was studied by McKee et al. (1984). They found that photoevaporation tends to homogenize a cloudy medium of mean density n_m out to a radius

$$R_h(t_{ms}) = 56 n_m^{-0.3} \text{ pc}, \tag{7}$$

where

$$t_{ms} = 4.4\ 10^6 \left(\frac{N_i}{10^{49}\ \text{s}^{-1}}\right)^{-1/4} \text{yr}$$

is the main sequence lifetime, and N_i is the number of emitted ionizing photons per second. While the bubble evolves within the homogenized region it will have the "classical" radius found by Weaver et al. (1977):

$$R_2(t) = 27\, n_m^{-1/5} \left(\frac{L_w}{10^{36}\ \text{erg s}^{-1}}\right)^{1/5} \left(\frac{t}{10^6\ \text{yr}}\right)^{3/5} \text{pc}. \tag{8}$$

The subsequent bubble evolution depends on whether or not it reaches the homogenization radius

$$R_h(t) = 1.05 \left(\frac{t}{t_{St}}\right)^{4/7} R_{St}, \tag{9}$$

where

$$R_{St} = 66.9\, n_m^{-2/3} \left(\frac{N_i}{10^{49}\ \text{s}^{-1}}\right)^{1/3} \text{pc},$$

$$t_{St} = 6.5\ 10^6\, n_m^{-2/3} \left(\frac{N_i}{10^{49}\ \text{s}^{-1}}\right)^{1/3} \text{yr}.$$

If C_i is the isothermal sound speed in the H II region, one can introduce the quantity

$$L_{St} = 4\pi R_{St}^2 \rho_m C_i^3$$

and define $L_w^* \equiv L_w / L_{St}$, $R^* \equiv R/R_{St}$, and $t^* \equiv t/t_{St}$. It is then possible to rewrite Eqs. (8)–(9) in an adimensional form

$$R_h^* = 1.05 t^{*4/7},$$

$$R_2^* = 1.46\, L_w^{*1/5} t^{*3/5}.$$

McKee et al. (1984) showed that if $L_w^* \ll 1$ an homogeneous bubble is confined by the ambient H II region: then $R_2 < R_h$ and Eq. (8) is valid at any time. For $L_w^* \leq 1$, the bubble expands to the edge of the homogenization radius. Clumps are overtaken by the hot bubble and start to cool: radiative losses reduce the pressure in the bubble and slow its expansion; it is therefore expected $R_2 \sim R_h$, an expansion intermediate between the energy-conserving and the momentum-conserving case.

In our case (see below) we have $L_w^* = 0.26$, and we are allowed to neglect clumps in the CSM in our numerical simulation. However we conclude pointing out that we are concerned here with the late steady bubble rather than with its previous dynamical evolution. The large value of $R_h(t_{ms})$ in Eq. (7) tells us that even if $L_w^* \gg 1$ the bubble will reach a final state not far from that predicted by Weaver et al. (1977), independently by the intermediate stages. In summary, H II regions around O stars are likely to assume a ring-like aspect, with emitting photoevaporating clouds located between R_h and the ionization radius $R_i > R_h$. Inside R_h the H II regions are homogeneous and have central cavities created by stellar winds (cf. McKee et al., 1984).

3.6. *Numerical results*

We computed a bubble model choosing the same parameters used by Weaver et al. (1977) in order to compare our results ($\dot{M} = 10^{-6}\ M_\odot\ \text{yr}^{-1}$, $n_0 = 1\ \text{cm}^{-3}$, $L_w = 1.27\ 10^{36}\ \text{e.g s}^{-1}$, $V_w = 2000\ \text{km s}^{-1}$). In Figs. 1 and 2 the bubble variables are displayed at $t = 4.3\ 10^4$ yr and $t = 2\ 10^6$ yr respectively. At the time of Fig. 1 the external shell is already cooled and collapsed; the hot interior, however, is still not radiating and the external shock follows the expansion law given by Eq. (8). In Fig. 2 the bubble has reached a nearly steady state. The cavity pressure is

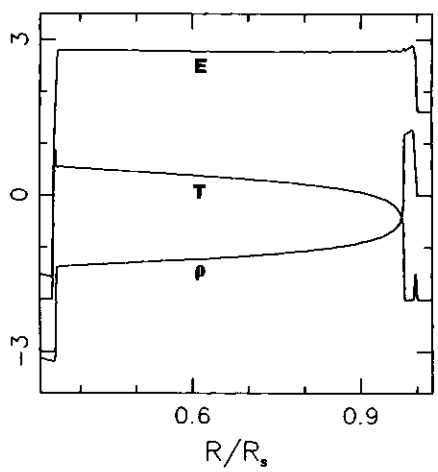

Fig. 1. Logarithmic plots of temperature, density and internal energy of an interstellar bubble for which $L_w = 1.27\ 10^{36}\ \text{erg s}^{-1}$ and $n_0 = 1\ \text{cm}^{-3}$ at time $t = 4.3\ 10^4$ yr. Values of T, ρ, E are normalized to 10^6 K, $1.67\ 10^{-24}\ \text{g cm}^{-3}$ and $10^{-13}\ \text{erg cm}^{-3}$ respectively. Distances are normalized to the outer radius $R_s = 4.5$ pc. Cooling is negligible at this time

© European Southern Observatory • Provided by the NASA Astrophysics Data System

'1989A&A...215..347C'

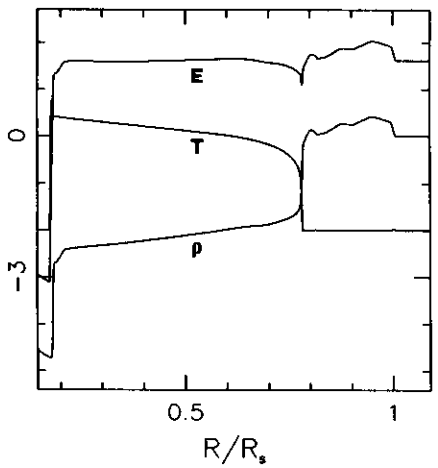

Fig. 2. The same as Fig. 1, but at $t = 2\ 10^6$ yr and $R_s = 50$ pc. The outer shell is not yet dissipated, but the conduction front is already stationary. Most of the stellar wind energy is radiated away. This cooling induces oscillations which originate at the conduction front

equal to that of the external H II region, and the relative thickness of the cold shell is increased; in fact the conduction front is steady while the external shock is slowing down to the sound speed dissipating in the external medium. At this time almost all the wind energy input is radiated away ($L \sim L_w$). The internal shock is located at $R_1 = 9$ pc and the conduction front at $R_b = 40$ pc; the hot cavity has a temperature $T \sim 3\ 10^6$ K and a numerical density $n < 10^{-2}$ cm^{-3}. All these values are in good agreement with those expected by semi-analytical calculations (Weaver et al., 1977). At late times, however, our solution develops oscillations which originate at the conduction front and propagate both through the external shell and in the hot cavity. As we have already remarked, when the cooling becomes important it occurs mostly close to the conduction front; here the evaporating gas passes through the temperature at which the cooling curve peaks ($\sim 2\ 10^5$ K), while being still relatively dense. With time the cooling tends to become higher than L_w. The pressure in R_b drops causing the inner shock to accelerate out. At the mean time the heat conduction is reduced (because more energy is now radiated away). But a reduction of the evaporating gas leads to a reduction of the cooling; the pressure in R_b increases and the inner shock is now decelerated. Weaver et al. (1977) do not find this effect. We think this due to the fact that, in order to speed up their computation, they adopt in their evolutionary equations a functional formula for the luminosity, which is connected with the integrated properties of the bubble and is independent from the position. We however are concerned with the general structure of the hot gas which is not significantly affected by such oscillations.

4. The supernova remnant

4.1. The model

The interaction between rapidly expanding supernova ejecta and the CSM gives rise to a pair of shocks; a blast wave expands out in the CSM, and the pressure of the shocked gas behind this drives a reverse shock in the stellar material. The shocked ejecta is separated by the compressed CSM by a contact surface through which the pressure and the velocity are continuous, while the density and the temperature may be not. If the CSM has a power law density profile ($\rho \propto r^{-s}$) as well as the external layers of the ejecta ($\rho \propto r^{-n}$) which are expanding homologously ($v = r/t$), the interaction region shows a self-similar behaviour. Such a behaviour was given by Chevalier (1982) who finds that the shock radii scale as

$$R_s \propto t^{(n-3)/(n-s)}. \tag{10}$$

Hydrodynamic calculations of supernova explosions find that $n \sim 9 \div 12$ (cf. Fransson, 1986 and references therein). The inner part of the ejecta (the core) is assumed to have an uniform density ρ_c up to a radius R_r where the power low density distribution starts to hold (the ramp). The self-similar solution remains valid as long as the inner shock radius is greater than R_r.

4.2. The adiabatic assumption

The Chevalier solution is valid if the fluid is supposed to be adiabatic, i.e. if the cooling time is longer compared to the flow time. Apart from the first months, when the Compton cooling is important (Fransson, 1986), the external shock is effectively adiabatic, essentially because of its high temperature. For the reverse shock the situation is more complicated due to its higher density and lower temperature, as well as the different chemical composition. For temperatures of some 10^7 K, typical of the reverse shock in the beginning, highly ionized metals are the most important coolants (Fransson, 1986 and references therein). The emission rate depends on the value of n, and the reverse shock may turn to be isothermal.

The high temperature gradients developed by the Chevalier solution could generate strong heat fluxes; also in this case the adiabatic assumption may become questionable. Bedogni and D'Ercole (1988) studied the effects of the electron thermal conduction on the SNR evolution by numerical simulations. They found that the flow looses its self-similar character becoming supersonic within the shocked ejecta, and multiple secondary shocks tend to form. The behaviour of the remnant depends on whether heat could be conducted through these internal shocks. If the thermal conduction is damped as soon as the induced perturbations grow out of the linear regime, the remnant can be effectively described by the adiabatic solution; the heat conduction only produces plasma turbulence on small scale. Bedogni and D'Ercole (1988) compared the X-ray brightness profile of Tycho's remnant with that expected by the Chevalier solution; the fit is quite good, apart for discrepancies in the internal region probably due to the Rayleigh-Taylor instabilities (see below). This means that in Tycho's SNR heat conduction is probably absent on large scale and that the interaction region behaves adiabatically. For this reason we do not include the thermal conduction in computing the remnant evolution.

4.3. Instabilities

Band (1988) worked out autosimilar solutions always considering homologously expanding ejecta with a power-law density gradient. These solutions, unlike Chevalier solutions, refer to isothermal or isentropic flows and in no case are energy-conserving. For a given set of n and s a family of solutions exists, each one having a different total energy; the sum of kinetic and internal energies in the interaction region does not equal in general the

© European Southern Observatory • Provided by the NASA Astrophysics Data System

'1989A&A...215..347C'

initial kinetic energy of the ejecta which have been incorporated into the interaction region. Although the total energy is not conserved, these solutions are however useful allowing, due to their autosimilar nature, a quite simple insight in cases where a fixed energy fraction is radiated away or absorbed by an unmodeled physical process such as turbulence.

As a matter of fact the Chevalier solutions present regions in which the pressure and density gradients have opposite signature, that means the fluid is Rayleigh-Taylor unstable in such regions (Chevalier, 1976). In particular, solutions for $s=2$ (which is the value expected for a remnant expanding in a steady wind) are unstable in the outer shell. Moreover the remnant may loose energy radiatively (especially in the reverse shock, as pointed out before) or through convection (see Band, 1988). It is therefore apparent that Band solutions may be useful to have a first overall picture of the remnant in cases of non negligible energy losses.

In the following, however, we will adopt the Chevalier solution as guiding model because of its simplicity. We will turn back on this argument in Sect. 6, when we shall present the results.

5. The strategy

In order to compute the interaction between the SNR and the bubble, it would seem natural to use a grid which extends from the centre up to a radius $R_{j\max}$ equal to the radius R_2 that will be reached by the stationary bubble. Then, "turning on" a stationary wind in the centre, we could follow the evolution of a bubble until its final stage. Later on we could simulate an SN explosion depositing an adequate amount of energy in the first mesh (or in the first few meshes) either as thermal energy or in the form of kinetic energy. Unfortunately this simple approach to the problem is not very useful nor efficient. In fact in the beginning, when the young bubble is developing, most of the grid is useless, and to compute the solution at each grid point represents just a waste of time. The same happens when the supernova starts to expand; in this case the great majority of the grid is "occupied" by the stationary bubble. Such a stationarity renders once more meaningless the computation at every mesh. Moreover, a huge number of grid points would be necessary to get an appreciable spatial resolution of the interaction region between the SNR and the bubble. In fact the bubble extends over about 50 pc, while the SNR would have a thickness of nearly 3 pc when it starts to interact with the bubble in R_1.

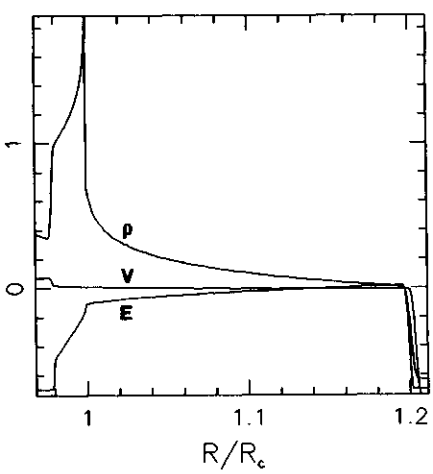

Fig. 3. The Chevalier solution for $n=8$ and $s=2$ obtained by our code. All the quantities are normalized to the outer postshock values

We therefore operated in a different way. We first computed the bubble evolution using a moving grid. Such a grid is just little larger than the distance between the inner and outer bubble shocks, and grows together with the bubble as it expands. In this way all the grid points are used and we obtain the maximum possible resolution at every time. Once the bubble reached a nearly stationary state, we started a new computation for the SNR adopting a separate grid and even a slightly different code; we in fact implemented the SLIC algorithm (Noh and Woodward, 1977) which allowed to follow exactly the contact surface between the shocked SN ejecta and the shocked wind. We started the second computation at $R=10^{17}$ cm, where the ramp of the ejecta was assumed to have the same density of the wind. Once again we used a moving grid to follow the interaction region which relaxed in short time towards the Chevalier solution.

As long as the SNR propagated into the unperturbed wind, the boundary conditions at the right hand side of the grid were given simply computating the physical quantities (such as density, momentum, etc.) of the wind in the last nodal point $R_{j\max}$. However, once the remnant approaches the inner side of the bubble in R_1, the external meshes of the 'supernova' grid overlap the inner meshes of the 'bubble' grid. Step by step $R_{j\max}$ crosses the bubble grid points R_k^b. The meshes of the SNR grid being smaller than that of the bubble, the evaluation of the boundary conditions in $R_{j\max}$ are obtained through a *remapping* of the bubble's variables over the last grid cell of the SNR. In other words the SNR grid does not 'see' the bubble, but realizes its presence through the boundary conditions. More details about these techniques are given in the Appendix.

6. Results

6.1. Presentation

In Figs. 4–7 we show the results obtained by our numerical computations assuming the explosion energy to be $E_0=10^{51}$ erg. The star which originated the bubble is assumed to have an initial mass about 20 $M_\odot$. Such a star is expected to lose nearly 10 $M_\odot$ during its life ($\sim 10^7$ yr). However pre-supernova star parameters such as $\dot{M}$ and N_i do not play a critical role provided that the star is earlier than B0. In this case in fact R_b does not depend on N_i [see Eq. (7)], while the bubble mass is determined by the gas evaporating from the cold shell rather than by the stellar wind material. The ramp of the ejecta was assumed to have a logarithmic slope $n=9$. We found that the overall dynamical interaction between the SNR and the bubble can be divided into four stages:

1) At $t=510$ yr the external shock of the remnant starts to interact with the bubble inner shock in R_1. Figure 4 shows the situation at three different times: $t=680$ yr, $t=910$ yr and $t=1334$ yr. It can be seen that a complicate situation develops in which several secondary shocks are created which interact each other and with the contact surface in R_c. This leads to a creation of a "cascade" of weaker and weaker discontinuities (either shocks or contacts). This situation lasts nearly 800 yr; actually at $t=1334$ yr the pressure (and the velocity) inside the interaction

© European Southern Observatory • Provided by the NASA Astrophysics Data System

'1989A&A...215..347C'

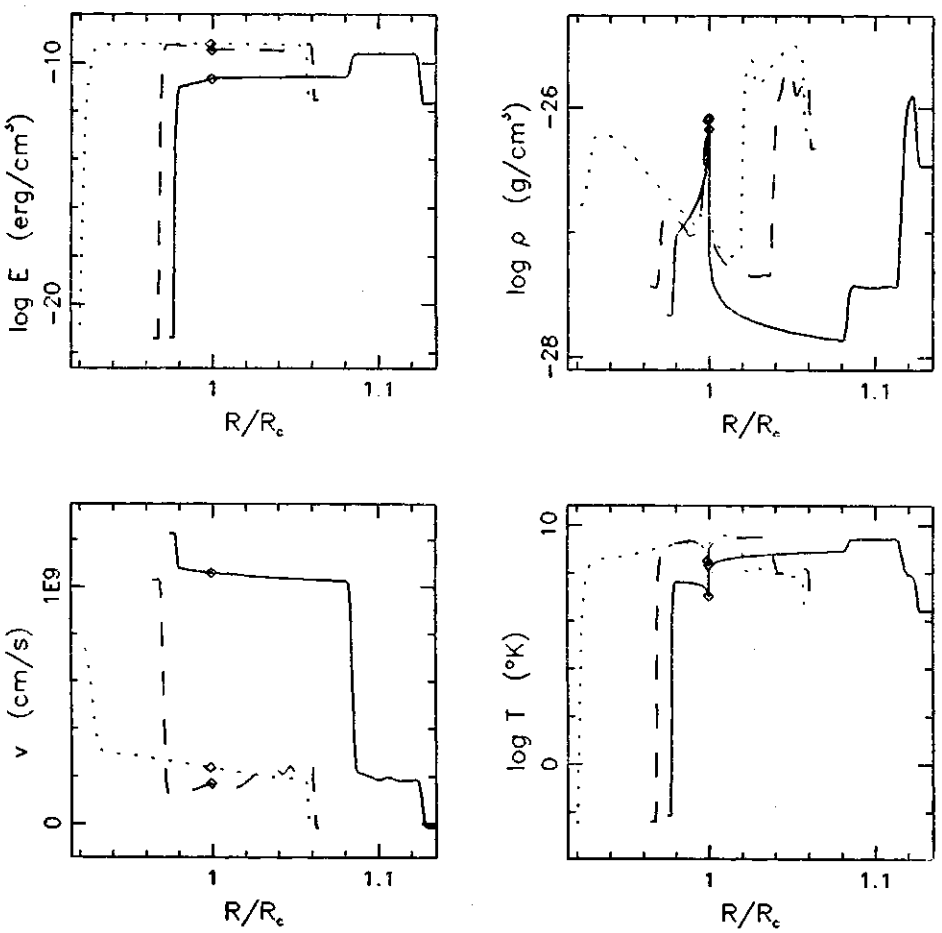

Fig. 4. The interaction of the SNR with the bubble at times $t=680$ yr, $t=910$ yr (dashed line), $t=1334$ yr (dotted line). Distances are normalized to the contact radius R_c between the ejecta and CSM. Values of R_c are 9 pc, 10.2 pc and 11.3 pc respectively. This figure shows the early stages of the interaction, until the pressure equilibrium is re-established

region turns back to an uniform distribution. The "re-equilibration" time is few times the sound crossing-time, as expected.

2) The second dynamical phase lasts 4700 yr and ends at $t=6000$ yr, when the top of the ramp reaches the reverse SNR shock. As shown in Fig. 5, during this phase the distribution of the variables tends to relax toward the "Chevalier-like" solution for $s=0$ (Chevalier, 1982). Actually, the radial density distribution inside the hot bubble follows a power law with $s=-1.23$. Chevalier (1982) has shown that for the autosimilar solutions the density at the contact can only tend toward 0 or ∞, depending on the sign of the ratio $b=[(sn-9)/\{(5-s)n+5s-21\}]$: for $b>0$ the density tends to be infinite. In our case $b<0$, and the density tends correctly toward 0 at the contact. It is worth-while to note that even choosing the maximum plausible value $n=12$ the qualitative behaviour of the solution does not change. Relaxation toward autosimilar solutions is a general behaviour. Had we chosen a Band solution to model the SNR propagating through the unperturbed wind, we should have obtained a "Band-like" solution.

3) Once the top of the ramp reaches the inner shock the fluid stops of course to relax toward the Chevalier solution. The reverse shock then slows down progressively and eventually reverts its velocity moving toward the centre; for a boundless wind the reverse shock would never reach the centre (Fabian et al., 1983), but in our case the presence of the bubble changes this behaviour. In this phase, therefore, the physical variables tend to relax toward the Sedov solution. Such a solution however is not achieved because the external shock reaches the conduction front when the inner shock is still quite far from the centre (Fig. 6). The contact between the outward shock and the conduction front occurs at $t=16000$ yr and represents the end of this third phase.

4) The outer SNR shock experiments a jump over two order of magnitude in the upstream density when it starts to interact with the exterior border of the hot bubble. The shock velocity decreases quite suddenly by a factor of ten because of its dependence by the square root of the unperturbed density; the result is a "stalling" of the outgoing shock which moves from $R=46.7$ pc to $R=48$ pc in the time interval between $t=76586$ yr and $t=101206$ yr. It results therefore that the shock velocity reduces to $5\ 10^6$ cm s^{-1}. At the mean time the external (with respect to the shock) temperature reduces by a factor of 100, so that the sound speed scales by a factor of ten. This means that the shock Mach number remains nearly inalterate. The most striking difference between this phase and all the previous ones is the formation of a cold radiating shell just behind the shock front. As shown in Fig. 7, this shell remains very thin (with a thickness of 0.2 pc) during all this stage which extends till $t=120000$ yr. By this time the external H II region recombines and the external pressure which confines the bubble reduces by a factor of 100, while the inner pressure is still high because the recombination time-scale is of order of $6\ 10^6$ yr. The SNR shock is therefore expected to become stronger. We however stopped our calculations here without taking into account these new external boundary conditions. The shell density is about $\rho_s=1.6\ 10^{-23}$ g cm^{-3}, with a

© European Southern Observatory • Provided by the NASA Astrophysics Data System

'1989A&A...215..347C'

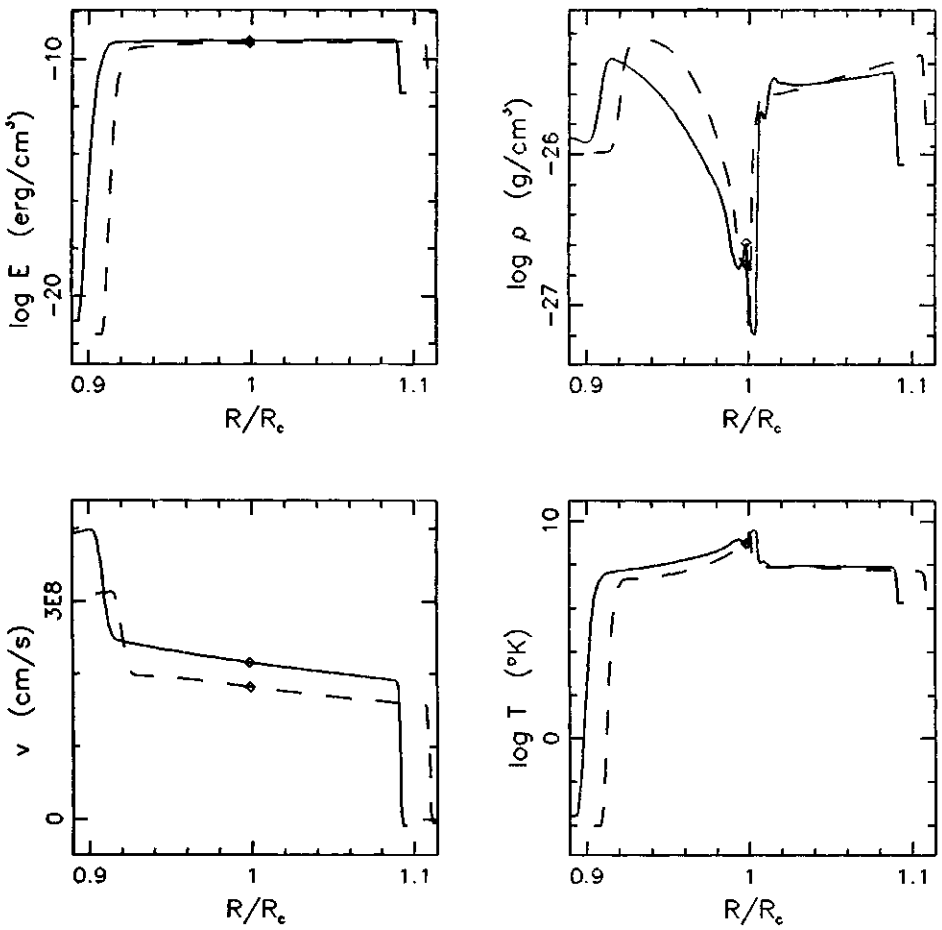

Fig. 5. The same as Fig. 4 but at $t=3605$ yr, $R_c=16.8$ pc and $t=6703$ yr, $R_c=22$ pc (dashed line). The solution is nearly autosimilar. Dashed lines represent the solution at the time when the top of the ramp reaches the inner shock

compression factor ~ 2.8, while the temperature becomes less than 10^4 K. Moreover, the inner shock reaches the centre at $t=40\,000$ yr, after that it is reflected outward once more (once the moving grid reached the centre we fixed the second grid point in $R=0$ and adopted reflecting boundary conditions in the first mesh). Later on a quite complex situation sets up, due to the interaction between the shock reflected by the origin and the shock reflected inward at the moment of the impact of the SNR with the boundary of the bubble in R_b. Several relatively weak shock waves criss-cross then all the region inside the cold thin shell. Because of the very low density inside this region, the dynamical effect of these shocks is not relevant and the overall structure of the region remains unchanged (see the density and temperature plots in Fig. 7).

6.2. *Scaling*

Unfortunately the computation of the bubble evolution is rather cumbersome because of the large number of grid points and the need to iterate several times at each time step to obtain the desired convergence in the heat transport algorithm. For this reason only the model presented above was computed. However, before discussing our results, it is worthwhile to try to generalize their validity as much as possible. Unfortunately neither the bubble evolution nor the subsequent SNR interaction present fully self-similar behaviour, and therefore there is no straightforward way to scale our present results on different values of the boundary conditions. On the other hand it is known that Eqs. (1a)–(1c) give the same solution if ρ is multiplied by a factor η, v by η^0, p (and E) by η, R and t by η^{-1}. This means that if we consider an unperturbed ISM with number density $n_0'=\eta n_0$ and a star mass loss rate $\dot{M}'=\eta^{-1}\dot{M}$ our results can be used to describe the interaction of an SNR with a bubble which is η times smaller, provided that all the values of the variables of our model are scaled as stated before. This scaling law is however rather restrictive because all the quantities must be scaled together; in particular, the mass of the ejecta scales as η^{-2}, representing a strong limit on the admissible variability range of η.

If however we disregard the first phase of the interaction which is rather confused and quite shortlived, it is possible to adapt our results to more general cases. As a matter of fact the ratio R_2/R_1 between the radii of the inner and outer shocks of the bubble varies with time and the flow is not self-similar; however, as long as $R_1 \ll R_2$ and the cooling is not effective, it is possible to find a self-similar solution to the bubble with an expansion law given by Eq. (8). It can be shown (Weaver et al., 1977) that this equation fits quite well even at later times, when the radiative losses are no more negligible. On the other hand we have shown that the remnant tends to relax toward the Chevalier solution "forgetting" the details of the interaction in R_1, and propagates following the time evolution given by Eq. (10). We may summarize the situation as follows: an "opaque" sphere exists whose radius is little larger than R_1. When the remnant shocks "emerge" from this sphere, the remnant itself can be roughly described by

© European Southern Observatory • Provided by the NASA Astrophysics Data System

'1989A&A...215..347C'

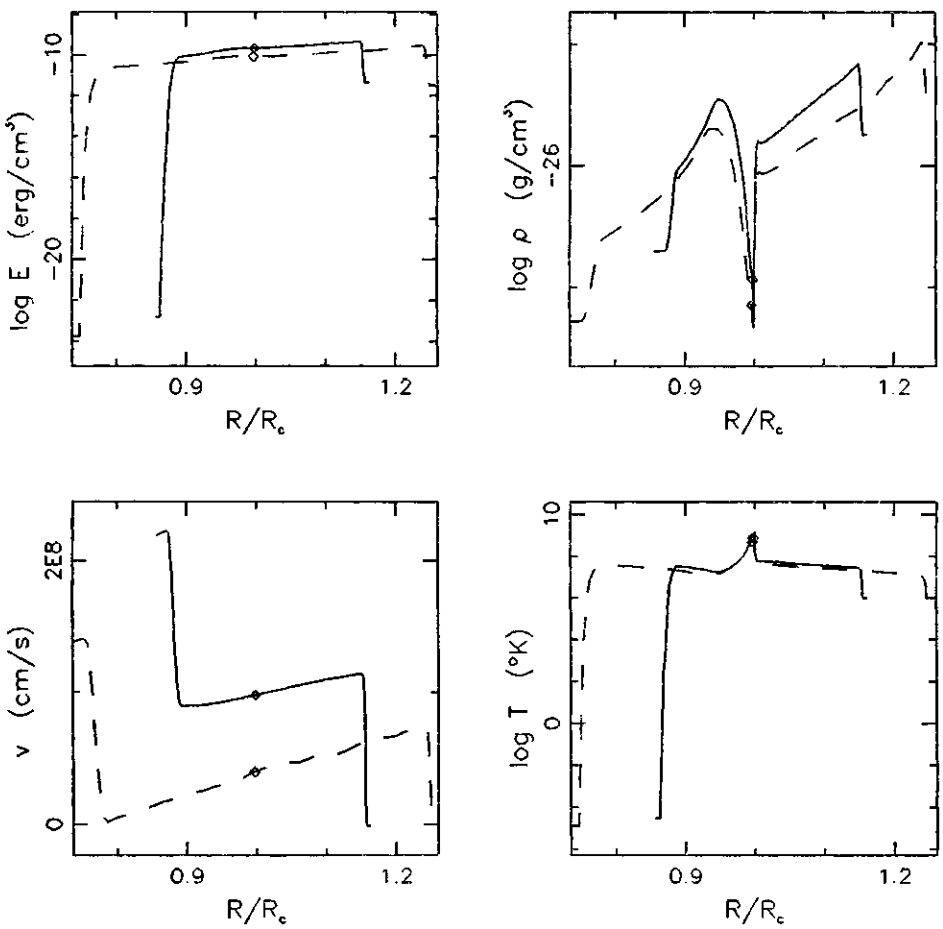

Fig. 6. The solution at time $t=10\,507$ yr, $R_c=28.4$ pc and $t=16\,409$ yr, $R_c=31.3$ pc (dashed line). Dashed lines show the solution at the time when the outer shock reaches the bubble conduction front. The maximum value attained by the dashed density curve is $\simeq 10^{-25}$ g cm^{-3}

the autosimilar solution given by Chevalier. Later on, when the top of the ramp of the ejecta density distribution reaches the inner shock, the solution tends to relax toward the Sedov solution.

One can define the time t_s at which the bubble stalls as the time when the pressure of the hot cavity equals the pressure of the outer H II region; adopting for the bubble pressure the relation given by Weaver et al. (1977) we have:

$$t_s \propto \left(\frac{L_w}{n_0}\right)^{1/2}. \tag{11}$$

Substituting t_s in Eq. (8) we obtain the radius of the stationary bubble,

$$R_b \propto \left(\frac{L_w}{n_0}\right)^{1/2}. \tag{12}$$

We write R_b instead of R_2 because at late times, when the thickness of the outer cold shell of the bubble is no more negligible, Eq. (8) refers to the conduction front rather than to the outer shock (which is slowing down in the ISM). Matching Eq. (12) to Eq. (10), we obtain after some tedious algebra the ratio τ between the time at which the outer remnant shock reaches R_b and the time at which the top of the ramp reaches the inner remnant shock:

$$\tau \propto L_w^{0.59} n_0^{-0.28}. \tag{13}$$

If $\tau > 1$ the Chevalier solution will break down before the remnant reaches R_b; for $\tau < 1$ it will hold until the edge of the cavity is reached. In our case $\tau = 2.7$, but Eq. (13) shows that for $n_0 = 35$ cm^{-3}, $\tau = 1$. Although these numbers must not be taken literally, Eq. (13) shows that for number densities of the unperturbed ISM higher than some tens the Chevalier solution never breaks down (before reaching R_b). In this case the description of the impact of the SNR against the inner side of the bubble shell will be different from that given in the previous Section.

One can ask now if it is possible that the Sedov solution is completely reached for some value of the parameters. Jones et al. (1981) show that the flow relaxes toward this solution when the mass of the compressed ISM is 8 times that of the ejecta; Fabian et al. (1983), discussing the Chevalier solution, found that for the case of an explosion in a constant density medium ($s=0$), the reverse shock reached the center when the swept up mass was 19 times that of the ejecta, illustrating that even at late times the structure can differ considerably from the Sedov case. In our calculations the ejecta have a mass of 10 $M_\odot$ and the mass inside the hot cavity is $M_b = 61\ M_\odot$; the ratio between these two masses is too small to get the Sedov solution. Going back once more to the paper of Weaver et al. (1977), and with the help of Eq. (11), we can scale M_b and the bubble density n_b as follows:

$$n_b \propto L_w^{-1/7} n_0^{6/7}, \tag{14}$$

$$M_b \propto L_w^{19/14} n_0^{-9/14}. \tag{15}$$

Equation (15) tells us that the Sedov case is never reached for any reasonable value of L_w and n_0.

© European Southern Observatory • Provided by the NASA Astrophysics Data System

'1989A&A...215..347C'

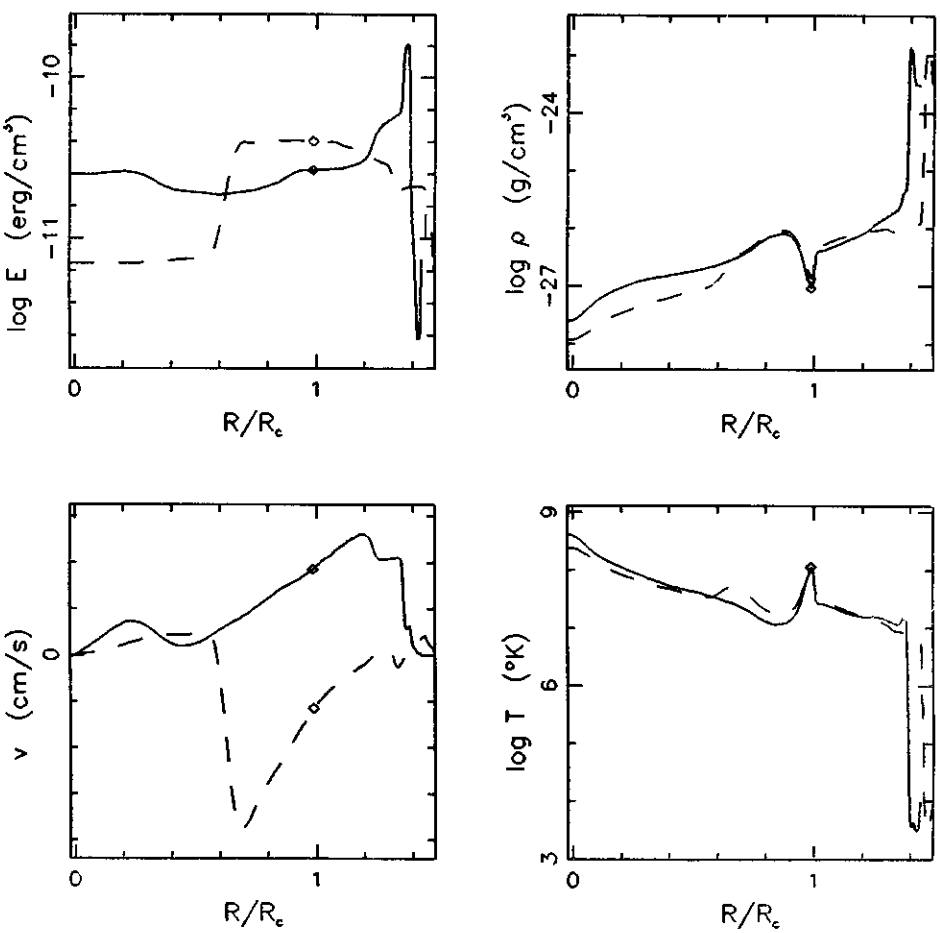

Fig. 7. The solution at time $t = 76\,586$ yr, $R_c = 33.6$ pc and $t = 101\,206$ yr, $R_c = 33$ pc (dashed line). A dense, cool shell is formed, while secondary shocks travel backward and forward from the origin to the shell. The minimum value attained by the dashed velocity curve is $\simeq -10^8$ cm s^{-1}

All the above considerations hold outside the "opaque" sphere stated before. The flow inside this sphere, at early times, is not influential for successive developments. Such a flow is important in young SNRs, but it depends critically on many factors we neglected in our computations, such as the slow wind in the RSG phase and possibly the mass loss during the WR stage (see however next section).

7. Discussion

As long as the SNR is expanding inside the hot cavity its emission measure is quite low (EM $< 10^{-2}$ cm^{-6} pc) due to the very low bubble density. Assuming as observability criterion at visual wavelengths the condition EM ≥ 50 cm^{-6} pc we conclude that the remnant cannot be detected inside the bubble. The situation is similar in the X-ray range. The thermal X-ray flux in the $1 \div 100$ keV region of the spectrum for SNRs is given by Gorenstein et al. (1974) as $L_X \sim 5\ 10^{33}\ n_0^2 R_{pc}^3$ erg s^{-1}. Using this expression for L_X and the X-rays measured for Pup A, the Cygnus Loop and the Vela SNR, one can conclude that an X-ray SNR is not observable if the ambient density is appreciably less than ~ 0.1 cm^{-3} (Kafatos et al., 1980). We conclude therefore that the SNR described in the previous section is not detectable as long as it expands inside the bubble. However, taking into account Eq. (14) and assuming $n_0 = 15$ cm^{-3} the remnant may become visible. Later on the external supernova shock reaches R_b: the outer region of the remnant cools and a thin cold shell forms with a compression ratio as high as ~ 2.8 (from a simple pressure balance argument however is possible to find that the compression factor is ~ 4 times higher: numerical computations give a smaller compression value due to the artificial viscosity which spread the thin shell somewhat). For higher external densities the compression factor increases, because in the isothermal case we have $\rho_s/\rho_0 \propto p/\rho_0 \propto E_0/(\rho_0 R_b^3)$. For $n_0 = 15$ cm^{-3} this value is ~ 44. Although the cold shell does not affect the SNR detectability in the X-ray range, it renders more favourable the SNR observation in visible light. The emission measure of the cold shell in our model is (following the recipe given by Kafatos et al., 1980) EM ~ 1 cm^{-6} pc, still too low for detection. The situation is expected to be more favourable for $n_0 = 15$ cm^{-3} because the emission measure in the cold shell would be higher.

The ISM has several phases; the dominant one is the hot ($T \sim 10^6$ K) tenuous ($n \sim 10^{-2}$ cm^{-3}) intercloud medium (ICM) with a volume filling factor f possibly as high as $\sim 80\%$. Because of such a low density it is believed that middle aged SNRs become detectable when they collide with a neutral cloud or clouds. Shull et al. (1985) model the evolution of SNR N49 assuming an early B star as progenitor. They found that atomic clouds are dispersed within the Strömgren sphere; this evaporating gas crosses the boundary of the H II region, recombining and creating a dense shell around it. Molecular clouds remain essentially undisturbed. The SN ejecta then propagate faster and substantially further through the less dense ICM, leaving behind the cool, more dense clouds. The expanding SN shock generates hard X-rays in the

© European Southern Observatory • Provided by the NASA Astrophysics Data System

'1989A&A...215..347C'

rarefied interior to the shell and drives optically radiating shocks into the molecular clouds. Such a model describes quite well the observed properties of N49, in particular the presence of bright clumps, 1–2 pc in diameter, which are distributed throughout the confines of the dense shell.

This is not the general picture of the Cygnus Loop (middle-aged SNR, $\sim 16\,000$ yr). While the X-ray emission is still consistent with a blast wave propagating into a medium of density $n \sim 0.1 \div 1\ \mathrm{cm}^{-3}$, optically the remnant is a filamentary nebulosity arranged in an incomplete shell with a diameter of nearly three degrees, no filament being found inside the shell as in N49. McKee and Cowie (1975) proposed that such filaments are dense clouds ($n \sim 2 \div 10\ \mathrm{cm}^{-3}$) in an inhomogeneous medium, which have suddenly decelerated the blast wave. The question rises however why the clouds are disposed in a spherical shell. McCray and Snow (1979) stressed that such a shell was created by the progenitor of the supernova, and not by the supernova itself. Braun and Strom (1986a) found that the radially structured ionization zones and the apparent energy-diameter relationship very strongly suggest the existence of a high density shell which pre-dates the SNR. They, assuming the McKee et al. (1984) scenario for the H II regions around O stars, suggest that the SNR shell comes from the ring-like H II region surrounding the progenitor. They base this picture, among others, upon the observed X-ray plateau which extends to 20 to 30% larger radius than the bright filamentary shell; there is a notable absence within this external volume (as large as that of the shell) of high density clouds. Braun and Strom suggest therefore that the shell derives from the previous H II ring which contains high density clouds. Equation (7) gives the radius R_h which separates the homogenized H II region from the ring-like cloudy structure. It turns out that n_m must be as high as 212 cm^{-3} to obtain $R_b \sim 11$ pc, which is the Cygnus radius at the revised distance (by Braun and Strom, 1986b) $D \sim 460$ pc; such a density seems too high for the Cygnus Loop environment. Actually H I shells are expected quite further, at the ionization radius $R_i > R_b$ as a result of the condensation of the gas evaporated from the inner clouds; in any case interstellar clouds remain present just outside these shells, in contrast with Cygnus Loop X-ray data.

Charles et al. (1985) also suggest that models based on uniformly evaporating clouds inside the remnant are ruled out by X-ray observations. In these models, in fact, the X-ray temperature is expected to increase with distance from the center (Cowie et al., 1981; Chieze and Lazareff, 1981), in conflict with what is observed. Furthermore, if clouds were uniformly distributed in the ambient medium prior to the SN explosion, the prominent limb brightening resulting in X-ray and optical images could not be explained. Charles et al. (1985) propose therefore that the Cygnus supernova was a Type II SN exploded inside a stellar wind bubble and H II region created by an early-type progenitor. They also, however, associate the bright ring of the Loop with the clouds that are expected close to R_h. Yet, the absence of clouds outside the Loop cannot be explained. Moreover, these authors propose a star of mass below 20 $M_\odot$ (say = 15 $M_\odot$) as progenitor of the Cygnus SN. In fact, as stated by Eq. (7), stars of spectral type B0 or earlier homogenize the ambient medium out to a distance which is too large in front of the Loop radius (~ 20 pc assuming the conventional distance of 770 pc). In our opinion it is not correct to extrapolate the results of McKee et al. (1984) to stars later than B0, because the flux of ionizing photons (as well as the wind luminosity L_w) drops abruptly. Effectively, as described before, such stars can better explain SNRs such as N49.

Although in accord with the previous authors, we disagree with regard to the details about the origin of the shell. From all the above we believe that cavity geometry rather than shell geometry is expected to dominate around O type SN progenitors.

When the bubble stalls, we have $R_b < R_h$ for any reasonable value of n_0 ($\equiv n_m$), while the outer shell dissipates giving rise to a cavity geometry; moreover the volume outside such a cavity does not contain clouds up to the radius R_h. It would be tempting to associate the bright filaments observed in Cygnus Loop with the cold shell which forms in our model when the external SNR shock hits the cavity boundary in R_b. Assuming $n_m \sim 15\ \mathrm{cm}^{-3}$, we have $R_h = 25$ pc, $n_b \sim 0.1\ \mathrm{cm}^{-3}$ and $R_b = 10.7$ pc, in good agreement with the Cygnus Loop radius (at a distance $D = 460$ pc). Filaments would be the product of Rayleigh-Taylor as well as thermal instabilities in the shell (McCray et al., 1975). Our present computations, however, cannot be directly adapted to the Cygnus Loop. The X-ray spectrum of this remnant is reasonably well fitted by a single temperature thermal plasma with $T \sim 2\ 10^6$ K, while the temperature in our model is $\geq 10^8$ K. Such a high temperature is an inescapable feature of the model, since the medium through which the shock propagates (i.e. the hot cavity) is already at $T \sim 3\ 10^6$ K. Now $T_b \propto (L_w n_0)^{1/7}$ and remains essentially the same for any acceptable value of n_0. On the other hand, once the blast wave has crossed the bubble interior, we have approximately $T \propto E_0/M_b \propto E_0 n_0^{9/14}$, so that the temperature rises with increasing n_0. A rarefaction wave which reaches R_b before the remnant seems the only way to lower T_b, the cooling time being too long ($\sim 7.1\ 10^6$ yr for $n_b = 0.1\ \mathrm{cm}^{-3}$). Such a wave in fact must be expected if the time spent by the SN progenitor in the red giant phase is not negligible as compared to the sound crossing time inside the bubble. In this case, indeed, the slow wind of the red giant cannot "sustain" the bubble, whose gas starts to move inwards while a rarefaction wave moves outwards at the local sound speed. The sound velocity inside the bubble, $c_b \propto T_b^{1/2} \propto (L_w n_0)^{1/14}$, is quite insensitive to the bubble parameters; the sound crossing time is given by $t_b = R_b/c_b = 4.4\ 10^3\ R_b(\mathrm{pc}) = 1.56\ 10^{-13}\ [(L_w/\mathrm{erg\,s^{-1}})\ (\mathrm{cm}^{-3}/n_m)]^{1/2}$ yr. For $n_m = 15\ \mathrm{cm}^{-3}$ we have $t_b = 3.4\ 10^4$ yr; this value represents an upper limit, having we assumed $R_1 \ll R_b$. Therefore, unless the Cygnus SN progenitor was a very massive star with an RSG life-time much less than $t_b = 3.4\ 10^4$ yr, the propagation of the rarefaction wave must be taken into account. While the rarefaction wave travels through the cavity, the bubble gas moves toward the centre and eventually interacts with the slow wind expanding from the central red giant. In summary, the bubble back-filling seems to influence the evolution of young as well as middle-aged SNRs (Ciotti and D'Ercole, in preparation).

8. Conclusion

We investigated the evolution of an SNR inside a bubble generated by the progenitor star. It can be shown (Shull et al., 1985) that the ionizing flux from B stars is not able to evaporate molecular clouds present in the cloudy CSM. Assuming the mechanical luminosity of such a star due to the stellar wind to be $L_w \sim 10^{32}\ \mathrm{erg\,s^{-1}}$, the pressure of this wind becomes negligible at a distance less than ~ 1.6 pc. From all the above, SNRs generated by B stars explosions are expected to expand through a cloudy H II region not affected by the previous stellar wind. The supernova blast wave travels adiabatically at high speed through the

© European Southern Observatory • Provided by the NASA Astrophysics Data System

'1989A&A...215..347C'

diffuse H II gas, driving radiative shocks into the clouds. Eventually the shock reaches the Strömgren radius where a dense neutral shell is present producing soft X-rays as well as optical emission from such a shell. This picture fits quite well SNRs such as N49 (Shull et al., 1985), but cannot describe remnants like the Cygnus Loop, which shows ring-like geometry with optical filaments disposed along the ring.

It is likely that the ring geometry derives from the previous action of the SN progenitor on the CSM. If this progenitor is assumed to be an O star, then the structure of the surrounding H II region is described by McKee et al. (1984). The ionizing photons of the central star (during its permanence on the main sequence) homogenize the medium up to a radius R_h, while observable clouds are confined between R_h and the ionization radius R_i giving rise to a visible ring structure. Braun and Strom (1986b) claim that this structure is responsible for the optical filaments geometry. We studied in some detail the dynamical evolution of an SNR from an O type star explosion, and suggest a different picture from that proposed by Braun and Strom.

Assuming a stellar wind with $L_w \sim 10^{36}$ erg s^{-1}, its effects on the surroundings must be taken into account. The action of the wind creates a bubble, an hot dilute gas bounded by a dense, relatively cold shell. When the internal pressure of the bubble equals the exterior H II pressure, the bubble stalls; the external shell becomes sonic and dissipates, while the hot cavity extends up to a radius $R_b < R_h$. We performed numerical computations for the bubble adopting the same parameters ($L_w = 1.27\ 10^{36}$ erg s^{-1}, $n_0 = 1$ cm^{-3}) used by Weaver et al. (1977), in order to compare our numerical results with their semi-analytical solution. Successively we simulated the SNR remnant expansion assuming the Chevalier solution (1982) to be valid as long as the remnant moves through the wind, before interacting with the bubble. In doing so we assumed that the fast wind blows until the star explodes; this in turn means that the RSG phase is negligible as compared with the BSG stage. Such an assumption allows us to consider the bubble stationary until its interaction with the SNR. This simplification may be valid for very massive stars ($M \geq 60\ M_\odot$) or for less massive, less metallic stars ($Z \sim Z_G/4$). If one wants to consider stars in more usual mass ranges, this assumption must be relaxed and the bubble back-filling must be accounted for.

We find that after a short-lived confused phase subsequent to the interaction between the remnant and the inner bubble shock, the solution tends to relax toward the Chevalier solution for $s = -1.2$ (the logarithmic slope of the density distribution inside the bubble). In this phase the remnant is hardly detectable due to low densities found inside the bubble. The SNR eventually reaches R_b where a huge escarpment in density is found. The shock quickly decelerates forming a dense ($n \sim 10$ cm^{-3}), cold ($T \sim 10^3$ K) shell; such a shell may have an emission measure high enough to be detected, depending on the parameter values. We therefore suggest that the shell in the Cygnus Loop is generated by the remnant, such a formation being however influenced by the previous interaction of the progenitor with the CSM. Although this picture seems to have general validity, our present calculations must be carried further on for a complete description. In fact, in its present form, the previous model suffers several drawbacks:

a) The shell of gas outside the bubble should have a density above 15 cm^{-3} since it was compressed by an ionization shock front, yet analysis of the optical shock emission gives a density below 15 cm^{-3} (Cox, 1972).

b) A second problem which we have not yet addressed is the mass of the dense shell M_s ($\sim 1200\ M_\odot$ in our computations). If the shell thickness is proportional to its radius, it is easy to see from a pressure balance argument that its mass is invariant to the scaling law. Such a mass has not been observed at 21 cm (DeNoyer, 1975).

c) The SNR expansion produces too high temperatures ($\sim 10^8$ K) as compared with observations ($\sim 2\ 10^6$ K); this comes from the fact that the shock while inside of the bubble expands through a hot gas.

About the first problem we can say that the scaling law should not be taken literally. In fact, as shown by Weaver et al. (1977), the value of the stalling radius is the half of the radius predicted by the autosimilar solution at the same time. This means that in reality the value $R_b \sim 11$ pc is attained for values of n_0 lower than 15 cm^{-3}. Alternatively, one can suppose that the central star explodes before the bubble becomes steady (which is likely to be true for sufficiently luminous O stars). In this case we may have relatively small bubble radii even for low unperturbed density.

As to point b), it is easy to show that ρ_s (and therefore M_s) does not change lowering n_0. In fact $\rho_s \propto p/c^2 \propto E_0/R^3$, which is independent of n_0 for a given shell radius. ρ_s, however, decreases with E_0. The usual value of E_0 given in literature for Cygnus Loop is in the range $2 \div 6\ 10^{50}$ erg; the shell mass obtained in our computation (assuming $E_0 = 10^{51}$ erg) may scale down to values lower than the detectability limit value ($\sim 340\ M_\odot$, DeNoyer, 1975).

Finally, referring to the temperature problem, we stress that, the cooling time being too long, the only way to lower the bubble temperature before the shock passage is given by the expansion of a rarefaction wave. Such a wave is expected if the RSG stage of the progenitor lasts for a period equal or longer than the sound crossing time t_b of the bubble. In this case, in fact, the missing support from the fast wind of the BSG phase induces a back filling of the bubble gas while a rarefaction wave propagates foreward. Since t_b is quite short ($\leq 10^5$ yr) in front of the usual RSG lifetime, this means that bubble "relaxation" must be considered. Moreover, the inflowing gas must eventually interact with the slow wind expanding from the central star. We therefore expect that a complete dynamical study of the CSM during the RSG stage must produce some insight on the expansion of middle-aged as well young SNRs. Such a study will be the subject of our next paper.

Acknowledgements. We thank A. Renzini for helpful discussions. We are also indebted to the referee, C.F. McKee, for his numerous comments and helpful suggestions. This work was supported by M.P.I. 60%.

Appendix

As outlined in Sect. 5, the SNR realizes the presence of the bubble through the boundary conditions at the last grid point. Let $R_{j\,max}$ and $R_{j\,max-1}$ be the last two points of the SN grid, and R_k^b the $k-th$ point of the bubble's grid. We chose the mesh size of both grids in such a way that $\Delta R = R_{j\,max} - R_{j\,max-1} < R_k^b - R_{k-1}^b\ \forall k$. This last condition must remain true at any time during the supernova expansion. The bubble's grid had 800 mesh points, while the supernova grid, which extended over a quite smaller

© European Southern Observatory • Provided by the NASA Astrophysics Data System

'1989A&A...215..347C'

spatial interval, had 220 mesh points; it turned out that, with these numbers, the SN mesh size was always smaller than the bubble mesh size. For the sake of simplicity we assume that, at a given time t, the last SN mesh ($R_{j\max}-R_{j\max-1}$) is fully inside a bubble mesh $R^b_k-R^b_{k-1}$ (i.e. $R_{j\max}<R^b_k$ and $R_{j\max-1}>R^b_{k-1}$).

As shown elsewhere (Bedogni and D'Ercole, 1986) our code uses the control-volume formulation and, in addition to slab averages, independent slab-averages gradient values are employed to represent the distribution of the convected quantity. In order not to loose the information connected with the slope values of the bubble quantities, the "remapped" quantities in the last SN mesh must share their zero-th moment (that is, the slab integral) and their first moment (proportional to the slope) with the bubble quantities. If a distribution $X_{k-1/2}(\xi)$ is linear in the interval (R^b_{k-1}, R^b_k), the mean value in the subinterval ($R_{j\max-1}$, $R_{j\max}$) is given dividing by ΔR the zone integral

$$\int_{R_{j\max-1}}^{R_{j\max}} X_{k-1/2}(\xi)\,d\xi. \tag{A1}$$

The slope $S_{j\max-1/2}$ of the replaced distribution will be obviously the same as that of the bubble distribution, $S^b_{k-1/2}$.

In general, however, ΔR may contain a nodal point R^b_k. that is $R_{j\max-1}<R^b_k<R_{j\max}$. In this case the generalization of Eq. (A1) is given by

$$\int_{R_{j\max-1}}^{R^b_k} X_{k-1/2}(\xi)\,d\xi+\int_{R^b_k}^{R_{j\max}} X_{k+1/2}(\xi)\,d\xi. \tag{A2}$$

The slope in this case is obtained dividing by $\Delta R^{3/2}/12$ the first moment given by

$$\int_{R_{j\max-1}}^{R^b_k} \xi X_{k-1/2}(\xi)d\xi+\int_{R^b_k}^{R_{j\max}} \xi X_{k+1/2}(\xi)\,d\xi, \tag{A3}$$

provided that $-\frac{1}{2}<\xi<\frac{1}{2}$ in ($R_{j\max-1}$, $R_{j\max}$).

Our numerical method being explicit, the integration time-step is constrained by the well known Courant condition $\Delta t\le\min_j\{(R_j-R_{j-1})/(c_j+v_j)\}$, where c_j and v_j represent the sound speed and the fluid velocity inside the mesh (R_{j-1}, R_j). We however imposed a further limitation given by

$$\Delta t\le\frac{R^b_{k+1}-R_{j\max}}{V^g_{j\max}},$$

where $V^g_{j\max}$ is the velocity of the last grid point $R_{j\max}$. This means that, if at a given time it is $R^b_{k-1}<R_{j\max}<R^b_k$, the last supernova mesh cannot cross more than one bubble grid in one time-step. In this way no bubble grid point is "forgotten" and all the available information is taken into account.

References

Aller, L.H.: 1961, *The Abundances of the Elements*, Interscience, New York

Avedisova, V.S.: 1972, *Soviet Astron.-A.J.* **15**, 708

Band, D.L.: 1988, *Astrophys. J.* **332**, 842

Bedogni, R., D'Ercole, A.: 1986, *Astron. Astrophys.* **157**, 101

Bedogni, R., D'Ercole, A.: 1988, *Astron. Astrophys.* **190**, 320

Braun, R., Strom, R.G.: 1986a, *Astron. Astrophys.* **164**, 193

Braun, R., Strom, R.G.: 1986b, *Astron Astrophys.* **164**, 208

Brunish, W.M., Truran, J.W.: 1982, *Astrophys. J. Suppl.* **49**, 447

Bychkov, K.V.: 1979, *Soviet. Astron.-A. J.* **23**, 438

Campbell, P.M.: 1984, *Phys. Rev.* **30**, 365

Castor, J., McCray, R., Weaver, R.: 1975, *Astrophys. J. Letters* **200**, L107

Charles, P.A., Kahn, S.M., McKee, C.F.: 1985, *Astrophys. J.* **295**, 456

Chevalier, R.A.: 1975, *Astrophys. J.* **198**, 355

Chevalier, R.A.: 1976, *Astrophys. J.* **207**, 872

Chieze, J.P., Lazareff, B.: 1981, *Astron. Astrophys.* **95**, 194

Chiosi, C., Maeder, A.: 1986, *Ann. Rev. Astron. Astrophys.* **24**, 329

Cowie, L.L.: 1977, *Astrophys. J.* **215**, 226

Cowie, L.L., McKee, C.F.: 1977, *Astrophys. J.* **211**, 135

Cowie, L.L., McKee, C.F., Ostriker, J.P.: 1981, *Astrophys. J.* **247**, 908

Cox, D.P.: 1972, *Astrophys. J.* **178**, 143

DeNoyer, L.K.: 1975, *Astrophys. J.* **196**, 479

Fabian, A.C., Brinkmann, W., Stewart, G.C.: 1983, in *Supernova Remnants and their X-Ray Emission, IAU Symp.* **101**, eds. I.J. Danziger, P. Gorenstein, Reidel, Dordrecht, p. 119

Falle, S.A.E.G.: 1975, *Astron. Astrophys.* **43**, 323

Feldman, W.C., Asbridge, J.R., Bame, S.J.: 1974, *J. Geophys. Res.* **79**, 2773

Fransson, C.: 1986, *IAU Colloq.* No. **89**, ed. I.J. Danziger

Hillebrandt, W., Höflich, P., Truran, J.W., Weiss, A.: 1987, *Nature* **327**, 597

Humphreys, R.M., Nichols, M., Massey, P.: 1985, *Astron. J.* **90**, 101

Itoh, H., Fabian, A.C.: 1984, *Monthly Notices Roy. Astron. Soc.* **200**, 645

Jones, E.M., Smith, B.W., Straka, W.C.: 1981, *Astrophys. J.* **249**, 185

Kafatos, M.: 1973, *Astrophys. J.* **182**, 433

Kafatos, M., Sofia, S., Bruhweiler, F., Gull, T.: 1980, *Astrophys. J.* **242**, 294

Maeder, A.: 1981, *Astron. Astrophys.* **102**, 401

Maeder, A.: 1983, *Astron. Astrophys.* **120**, 113

McCray, R., Stein, R.F., Kafatos, M.: 1975, *Astrophys. J.* **196**, 565

McCray, R., Snow, T.P. Jr.: 1979, *Ann. Rev. Astron. Astrophys.* **17**, 213

McKee, C.F.: 1974, *Astrophys. J.* **188**, 335

McKee, C.F., Cowie, L.L.: 1975, *Astrophys. J.* **195**, 715

McKee, C.F., Van Buren, D., Lazareff, B.: 1984, *Astrophys. J. Letters* **278**, 115

Noh, W.F., Woodward, P.R.: 1977, in *Lecture Notes in Physics No. 59*, Springer, Berlin, Heidelberg, New York

Shull, P.Jr., Dyson, J.E., Kahn, F.D., Kim, A.W.: 1985, *Monthly Notices Roy. Astron. Soc.* **212**, 799

Spitzer, L., Jr.: 1962, *Physics of Fully Ionized Gases*, Interscience, New York

Steigman, G., Strittmatter, P.A., Williams, R.E.: 1975, *Astrophys. J.* **198**, 575

Weaver, R., McCray, R., Castor, J., Shapiro, P., Moore, R.: 1977, *Astrophys. J.* **218**, 377

Zel'dovich, Y.B., Raizer, Y.P.: 1967, *Physics of Shock Waves and High-Temperature Hydrodynamic Phenomena*, Academic Press, New York

© European Southern Observatory • Provided by the NASA Astrophysics Data System